Journal of Inorganic and Organometallic Polymers and Materials (2020) 30:388–399
https://doi.org/10.1007/s10904-019-01197-x

Biogenic Synthesis of Silver and Gold Nanoparticles from *Lactuca indica* Leaf Extract and Their Application in Catalytic Degradation of Toxic Compounds

Thanh-Truc Vo[1,2] · Chi-Hien Dang[2,3] · Van-Dat Doan[4] · Van-Su Dang[5] · Thanh-Danh Nguyen[1,3]

Received: 11 April 2019 / Accepted: 19 May 2019 / Published online: 25 May 2019

Abstract

The present study describes an eco-friendly approach for the synthesis of colloidal solution of silver and gold nanoparticles (L-AgNPs and L-AuNPs) from the aqueous extract of *Lactuca indica* leaf. Major parameters affecting on the formation of L-AgNPs and L-AuNPs were optimized using UV–Vis analysis at absorption maximum around 423 nm and 531 nm, respectively. The plant extract as reducing and capping agents of MNPs was demonstrated by Fourier-transform infrared (FTIR) spectroscopy. The nanoscale of metals was confirmed by Transmission electron microscopy (TEM) measurements. TEM studies revealed that L-AgNPs were mostly spherical with average size of 13.5 nm and L-AuNPs possessed multi shapes with an average size of 14.5 nm. Selected area electron diffraction (SAED) analysis and X-ray diffractometer (XRD) data confirm their crystalline structure. The nanomaterials showed efficient catalysis in the degradation of 4-nitrophenol and methyl orange.

Electronic supplementary material The online version of this article (https://doi.org/10.1007/s10904-019-01197-x) contains supplementary material, which is available to authorized users.

✉ Thanh-Danh Nguyen
danh5463bd@yahoo.com

[1] Institute of Research and Development, Duy Tan University, Da Nang City, Viet Nam

[2] Graduate University of Science and Technology, Vietnam Academy of Science and Technology, 18 Hoang Quoc Viet, Cau Giay, Hanoi, Viet Nam

[3] Institute of Chemical Technology, Vietnam Academy of Science and Technology, 1 Mac Dinh Chi Street, District 1, Ho Chi Minh City, Viet Nam

[4] Faculty of Chemical Engineering, Industrial University of Ho Chi Minh City, Ho Chi Minh City, Viet Nam

[5] Department of Chemical Technology, Ho Chi Minh City University of Food Industry, Ho Chi Minh City, Viet Nam

Graphical Abstract

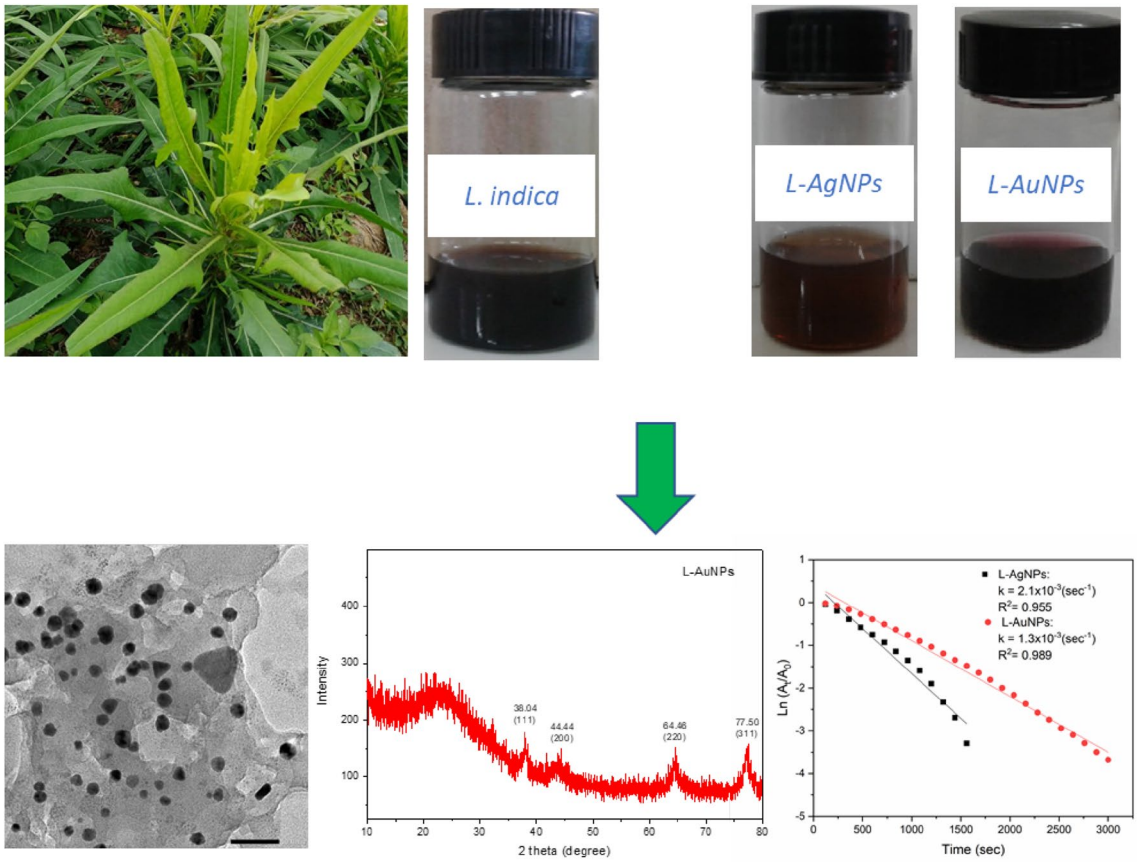

Keywords Biosynthesis · Silver nanoparticles · Gold nanoparticles · *Lactuca indica* · Pollutant degradation

1 Introduction

Due to especially interesting changes in the physicochemical properties at the nanoscale, the noble metallic nanoparticles (MNPs) have been particularly considered during the past decades [1, 2]. Numerous chemical and physical methods have been developed for synthesis of MNPs like silver nanoparticles (AgNPs) and gold nanoparticles (AuNPs). However, these approaches are often used the toxic substances harmful to the environment and required expensive conditions such as high temperature and pressure [3, 4]. Green synthesis of MNPs can overcome the limitations of these methods. The enhancements of biosynthesis i.e. using microorganisms [5], algae [6] and plants [7] have led to developing an eco-friendly environment method for the synthesis of MNPs. Among them, biosynthesis using aqueous extract of plants as reducing and stabilized agents has been considered as environmentally benign alternative to physicochemical methods due to the biogenic MNPs possessed significant advantages in large-scale production such as cost efficiency, controllable size, high stability, and biocompatibility [8, 9].

Wastewater treatment for removal of toxic organic pollutants by catalysis of MNPs is a novel approach and an alternative to other chemical methods. For instant, Choudhary et al. [10] have successfully synthesized AuNPs based on aqueous extract of *F. vulgare* seeds and efficiently applied for degradation of anthropogenic dyes. Reduction performance of the various dyes has been investigated in the presence of AgNPs biosynthesized from *S. acuminata* fruit extract [11]. Size and shape of AuNPs biosynthesized extract of *A. assamica* leaf have been controlled by varying the concentrations of metal ion and extract [12]. Most recently, Bonigala et al. have greenly synthesized AgNPs and AuNPs catalysts from aqueous extract of *S. tuberosa* [13]. As a result, biogenic noble MNPs are potential candidates for effective industrial application of contaminant treatment.

Lactuca indica leaf is well known as a folk medicine in Asia. Aqueous extract of *L. indica* leaf has been popularly used in treatment of various diseases including in

antioxidant, antibacterial applications and anti-inflammatory [14]. Aqueous extract of *L. indica* leaf contained polyphenolic compounds such as flavonoids and phenolic acids [15, 16] that is major responsibility for biosynthesis of MNPs. To the best of our knowledge, the aqueous extract of *L. indica* leaf has not been investigated for synthesis of MNPs. Herein, we present an eco-friendly method for the low-cost synthesis of AgNPs and AuNPs based on the aqueous extract of dried *L. indica* leaf as reducing and capping agents. The potential applicability of these MNPs is demonstrated by catalytic degradation of 4-nitrophenol and methyl orange, typically resistant organic contaminants in the environments.

2 Materials and Methods

2.1 Materials

All chemicals used were of analytical grade and utilized without further purification. Silver nitrate, hydrogen tetrachloroaurate (III) hydrate, Sodium tetrahydridoborate ($NaBH_4$), methyl orange and 4-nitrophenol were purchased from Acros (Belgium).

2.2 Preparation of *L. indica* Leaves Extract

The *L. indica* leaf purchased Khai Minh Macrobiotics (Ho Chi Minh city) was dried in the air and ground to obtain a fine powder by using an electronic blender. The resulting powder (10 g) were placed into a double-neck round bottom flask and then boiled at reflux with the distilled water (100 mL) for 1 h. The obtained extract was filtered and stored at 4 °C for further studies.

2.3 Biosynthesis and Optimization of L-AgNPs and L-AuNPs

The biosynthesis of MNPs was carried out with the solution of $AgNO_3$ and $HAuCl_4$ and aqueous extract of *L. indica* leaves under continuous stirring at 1200 rpm and dark condition to avoid unnecessary photochemical reactions. Changes in the color of the reaction mixture observed were inferred that MNPs were successfully synthesized. Then the MNPs were separated from solutions by centrifugation at 4000 rpm for 20 min. The clear supernatant was discarded and the solid MNPs were washed thrice with triple distilled water to remove unconverted metal ions and the unreacted phytoconstituents. For further studies on physicochemical characterization and catalytic activity, the dry powders of MNPs were obtained after drying at 90 °C for overnight. For their reproducibility, reaction parameters were optimized. The reaction mixture stirred on a magnetic stirrer at different concentration of metallic ions (in range of 0.5–2.0 mM), temperature (in range of 30–120 °C), and reaction time (in range of 0–140 min). The optimization of conditions was explored through measurement of UV–Vis spectra in the range of 200–800 nm which can increase absorbance at the peaks of around 400 nm for biosynthesis of AgNPs and 540 nm for biosynthesis of AuNPs. MNPs prepared by the optimized condition were used to study characterizations and their applications.

2.4 Characterization of L-AgNPs and L-AuNPs

UV–Vis spectra were measured at room temperature on a Jasco Spectrometer V-630 spectrophotometer (U.S.A) at the range between 200 and 800 nm wavelengths. For FTIR measurement, dried samples including *L. indica* extract and biosynthesized MNPs were ground to fine powder, then measured on a Tensor 27 FTIR spectrophotometer (Brucker, Germany) in the range of 4000–500 cm^{-1}. To obtain the X-ray diffraction (XRD) pattern of the MNPs, the dried samples were analyzed using a Shimadzu 6100 X-ray diffractometer (Japan) operated at voltage 40 kV, current 30 mA with CuKα radiation of 1.5406 nm wavelength at a scanning rate 0.05°/s, step size 0.02θ over the 2θ range from 10° to 80°. Transmission electron microscopy (TEM) and high-resolution transmission electron microscopy (HRTEM) images were recorded on a JEOL JEM-2100 transmission electron microscope, operating at an accelerating voltage of 200 kV. Selected area (electron) diffraction (SAED) pattern of the nanoparticles was recorded. Field emission scanning electron microscopy (FESEM)–Energy dispersive X-ray spectroscopy (EDX) analyzer (JEOL JSM-7401F, Japan) was used to analyze chemical elements in micrometer area. The thermal properties of the MNPs were determined by the thermal analysis combining thermogravimetry (TG) analysis and different thermal analysis (DTA) using a LabSys evo S60/58988 Thermoanalyzer (France). The dried samples were heated from 30 to 800 °C with a heating rate of 10 °C/min in the air atmosphere.

2.5 Catalytic Activity of L-AgNPs and L-AuNPs

The catalytic ability of L-AgNPs and L-AuNPs was exploited for removal of pollutants including (4-NP) and methyl orange (MO) using reducing agent $NaBH_4$ at the room temperature as a model reaction accordingly previous literatures with necessary modifications. The pollutants (2.5 mL, 0.1 mM) mixed with $NaBH_4$ (0.5 mL, 0.1 M) and then added into a quartz cell (1 cm path length). The MNPs (1 mg) was added forwards the reaction mixture after completion of the washing process with ethanol. Control experiments were also executed without the catalysts. The catalytic performance and kinetics of the degradation reactions were investigated by monitoring the UV–Vis

absorbance spectra in a time-dependent manner in a scanning range of 200–800 nm. A rapid decrease in absorbance of 4-NP and MO in the UV–Vis spectra might be observed at peaks of 400 and 464 nm, respectively. For study on catalytic degradation kinetics, because this work used amount of $NaBH_4$ exceeded that of the pollutants, the concentration of $NaBH_4$ stayed practically constant throughout the course of the reaction. Thus, the reaction can be considered as a pseudo first-order reaction which its reaction kinetic can be described by the equation $\ln(A_t/A_0) = -kt$, where k is a rate constant, t is the reaction time, $[A_0]$ is the initial concentration of the pollutants and $[A_t]$ is the concentration at time 't' [17]. Therefore, it follows that a plot of ln [A] versus time yields a straight line and from the slope of the line, k can be determined.

3 Results and Discussion

3.1 Biosynthesis of L-AgNPs and L-AuNPs

Aqueous leaf extract of the important medical plant *L. indica* which contains large content of phenolic antioxidants responsible for the reduction of MNPs, was used for the environmentally friendly synthesis of silver and gold nanoparticles. The route of this work is illustrated in Fig. 1. The leaf was dried in an oven and refluxed with triple distilled water for 2 h. The aqueous extract possesses a dark red color with an intensive absorption peak at 272 nm which might relate to $\pi \rightarrow \pi^*$ transition of phenolic compounds [14, 18]. The reduction process occurring to aqueous AgNO3 and $HAuCl_4$ was confirmed by the formation of brown and red color, respectively. UV–Vis spectra of the reaction medium were recorded during the synthesis of silver and gold nanoparticles. A peak was observed at 423 nm for L-AgNPs. This is characteristic of the surface plasmon resonance (SPR) of AgNPs. In case of gold, the SPR band was observed at 531 nm after the reduction process. Optimization of stable MNPs formation was carried out by change of the reaction conditions including concentration of metallic ions, reaction temperature and reaction time. After purification and collection using centrifugation technique, the biosynthesized MNPs are characterized by physicochemical analysis techniques and applied for evaluation of catalytic activities for degradation of 4-NP and MO.

3.2 Optimization of Reaction Parameters

In order to ascertain the formation of stable nanoparticles, UV–Vis spectrophotometry is an efficient method because colloidal solutions of AgNPs and AuNPs show the absorption bands of corresponding SPR. The change in absorbance and λ_{max} values gives an indication about concentration, size and morphology of the nanoparticles [19] which might

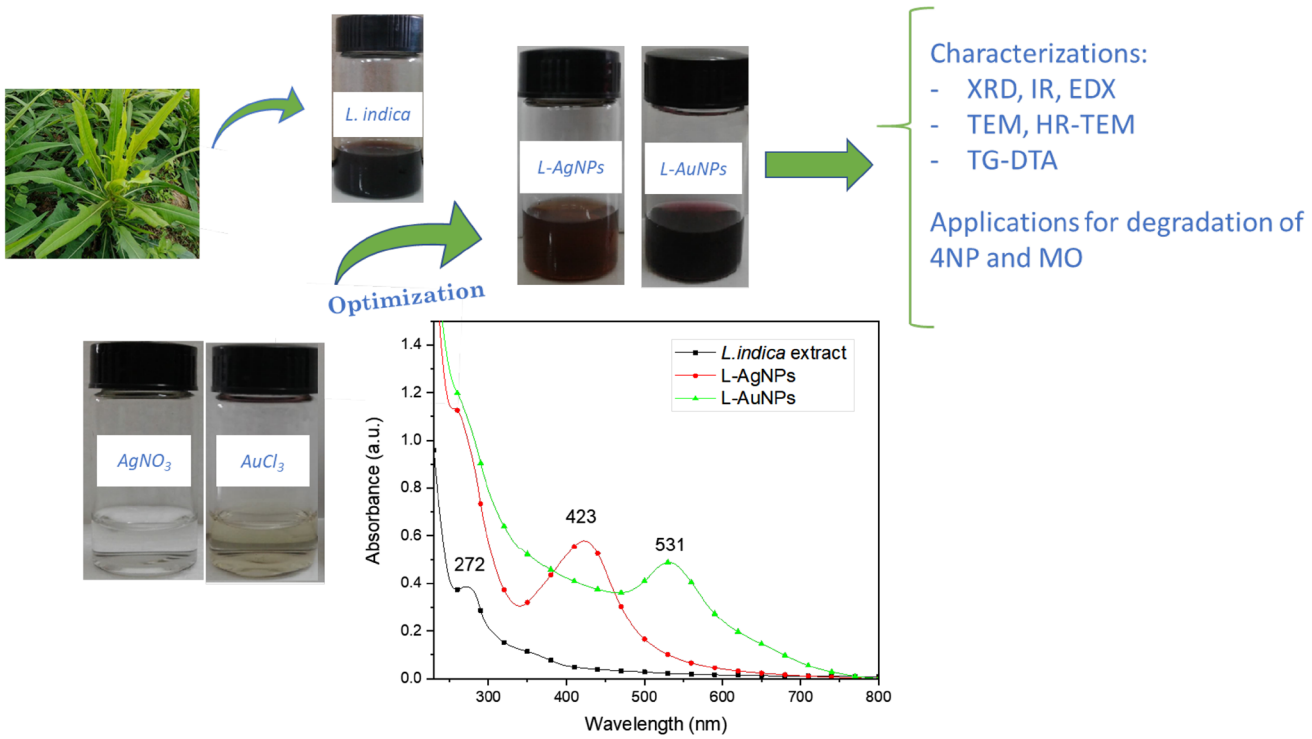

Fig. 1 schematic illustration of studies on L-AgNPs and L-AuNPs biosynthesized from *L. indica* leaf extract

depend on different reduction conditions. Thus, optimization of reaction condition is necessary to get insight in biosynthesis of MNPs using the aqueous extract of *L. indica* leaf. In the present study, various parameters like concentration of metallic ions, temperature, and incubation time are taken into consideration of investigation.

To know the effect of concentration of metallic ions on the synthesis of MNPs, different concentrations (0.5, 1.0, 1.5 and 2.0 mM) of both $AgNO_3$ and $HAuCl_4$ solutions were used to add into a constant volume of the extract. Increase of both metallic ion concentrations induced growth of absorbance at the corresponding SPR band. The optimum concentration was observed at 1.0 mM for the synthesis of L-AgNPs and 1.5 mM for the synthesis of L-AuNPs (Fig. 2a, b). When the metallic ion solutions were concentrated over the optimum concentrations, reduction of the absorbance values was clearly observed. The absorbance was lower in the case of high concentrations may be due to the agglomeration of

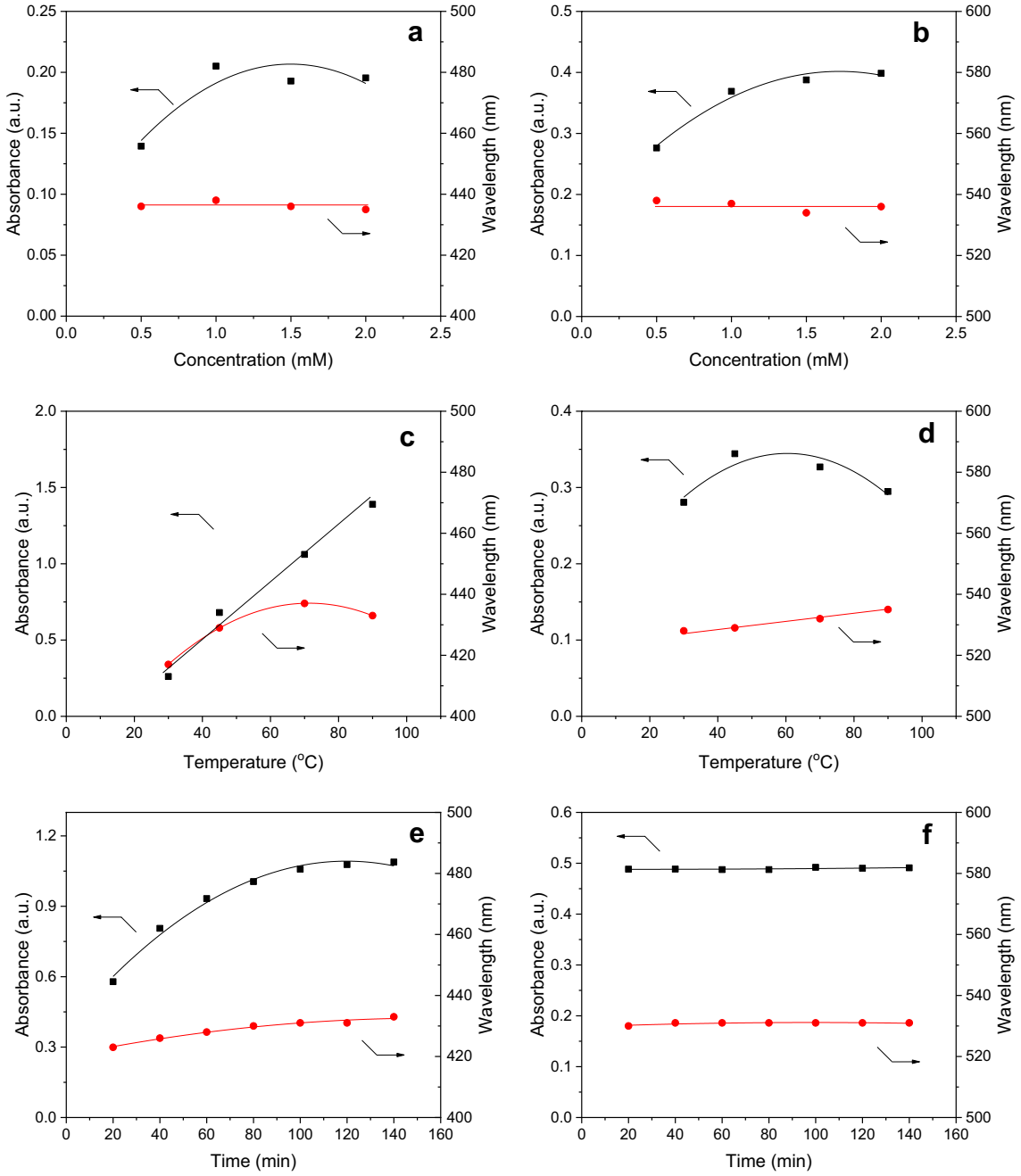

Fig. 2 Plots of parameters versus absorbance and wavelength values of L-AgNPs (left) and L-AuNPs (right): concentration of metallic ions (**a**, **b**), reaction temperature (**c**, **d**) and reaction time (**e**, **f**)

nanoparticles in the colloidal solution. In fact, the aggregation formed can be recognized during the reduction process at these concentrations. Meanwhile, almost no change in λ_{max} values of the SPR peak was observed when the salt concentration was concentrated. It leads to a notice that no effect of the metallic ion concentrations on the size and shape of MNPs formed. Based on performance of synthesis and stability of the nanoparticles in the colloidal solution, the optimum concentrations of the metallic ions were selected for further optimization.

In next step, the effect of temperature on biosynthesis is monitored by keeping the concentration of metallic ions constant and then change reaction temperature conditions in range of 30–90 °C. The different trends of temperature dependence in the synthesis of L-AgNPs and L-AuNPs are observed in Fig. 2c, d, respectively. In the biosynthesis of L-AgNPs, the results showed that increase of reaction temperature leads to acceleration of maxima intensity at SPR peak and changes in λ_{max} values. Otherwise, formation of AgNPs in the *L. indica* extract medium is strongly dependent on the reaction temperature. A maximum λ_{max} value and significantly high absorbance are found at 70 °C which may relate to the stable AgNPs colloidal solution. In contrast, the spectra of L-AuNPs showed optimum absorbance value at 45 °C and lower values might relate to the agglomeration of AuNPs at the higher temperatures. A slight red shift was found from 528 to 535 nm when the reaction temperature was increased from 30 to 90 °C.

For the evaluation of the reaction time, reaction mixture with an optimized concentration of metallic ions was stirred at 70 °C for L-AgNPs and 45 °C for L-AuNPs and measurement of UV–Vis spectra was carried out every 20 min. It is observed that the reaction started in initial 20 min after the addition of both the salt solutions. The results showed that the optimum reaction time for the AgNPs synthesis by aqueous extract of *L. indica* leaves was 100 min and a slight red shift could be found with increase of reaction period (Fig. 2e). It is noteworthy that the reaction time seems no effect on the formation of AuNPs after initial 20 min. In fact, both absorbance and λ_{max} values observed were constant with change of the reaction time. For further studies on their characterization and application, we have selected the optimum parameters such as $AgNO_3$ concentration of 1.0 mM, stirred at 70 °C in 100 min and $HAuCl_4$ concentration of 1.5 mM, stirred at 45 °C in 20 min.

3.3 FTIR Spectroscopy

FTIR spectra were measured to identify the possible functional groups of phytoconstituents in the *L. indica* extract. The FTIR spectra of dried aqueous extract, biosynthesized L-AgNPs and L-AuNPs are shown in Fig. 3. FTIR spectra of all the samples revealed the similar absorption bands, indicated that biomolecules of the *L. indica* extract might be stabilizing agents of MNPs. The phytochemical analysis of *L. indica* revealed the presence of triterpenoids, flavonoids and glycosides [14, 20, 21]. Peaks of *L. indica* extract are observed at 1015, 1109, 1384, 1446, 1632, 2854, 2923 and 3428 cm^{-1}. After the reduction of the salts, these characteristic peaks were shifted to the new positions at 1022, 1380, 1439, 1601, 2851, 2916 and 3428 cm^{-1} for L-AgNPs and 1031, 1382, 1449, 1647, 2855, 2924 and 3414 cm^{-1} for L-AuNPs. The broad bands at around 3400 cm^{-1} are assigned to O–H stretching vibration indicating the presence of glucosides while strong peaks at around 1450 cm^{-1} (stretching vibration of –C=C) and around 1020 cm^{-1} (stretching vibrations –C=O) suggests the presence of flavonoids adsorbed on the surface of metallic nanoparticles. It confirmed that the phytoconstituents present in the aqueous extract of *L. indica* leaf were responsible for the reduction of the metallic ions and stabilization of MNPs.

3.4 X-ray Diffraction Analysis

The structural information of the biosynthesized MNPs is characterized by using powder XRD spectra as shown in Fig. 4. From XRD data, their average particle size was determined using Debye–Scherrer equation, $[d = 0.9\lambda/\beta\cos\theta]$ where 'd' is the mean diameter of the particles; 'β' is $(\pi/180) \times$ FWHM; 'λ' is the X-ray radiation source (0.1540 nm) and 'θ' is the Bragg angle. The patterns clearly showed the Bragg peaks at (2θ) 38.12°, 44.26°, 64.18° and 77.02° for L-AgNPs and 38.04°, 44.44°, 64.46° and 77.50° for L-AuNPs which corresponds to the (111), (200), (220) and (311) crystallographic planes, respectively [13]. It reveals that the AgNPs and AuNPs grow in a face-centered cubic (FCC) fashion. The most intensive peak from L-AgNPs and L-AuNPs was from the (111) plane, indicated the preferred orientation of the crystals towards the (111) plane. By determining the width of (111) reflection of MNPs, the average crystalline size of the AgNPs and AuNPs is estimated to be 12.0 nm and 9.34 nm, respectively. In additional, the unidentified peaks (2θ) such as 31.46° and 46.86° appeared in both the spectra of MNPs might reveal the presence of the organic compounds in the *L. indica* extract. Similar results were also observed from the literatures [22, 23].

3.5 EDX and TEM Analysis

The morphology, dimension and distribution of the biosynthesized MNPs were observed using microscopic analysis. Figures 5 and 6 described TEM, particle size distribution, HRTEM, SEAD pattern, and EDX data of L-AgNP and L-AuNP, respectively. L-AgNPs showed a roughly spherical geometry in a particle size distribution

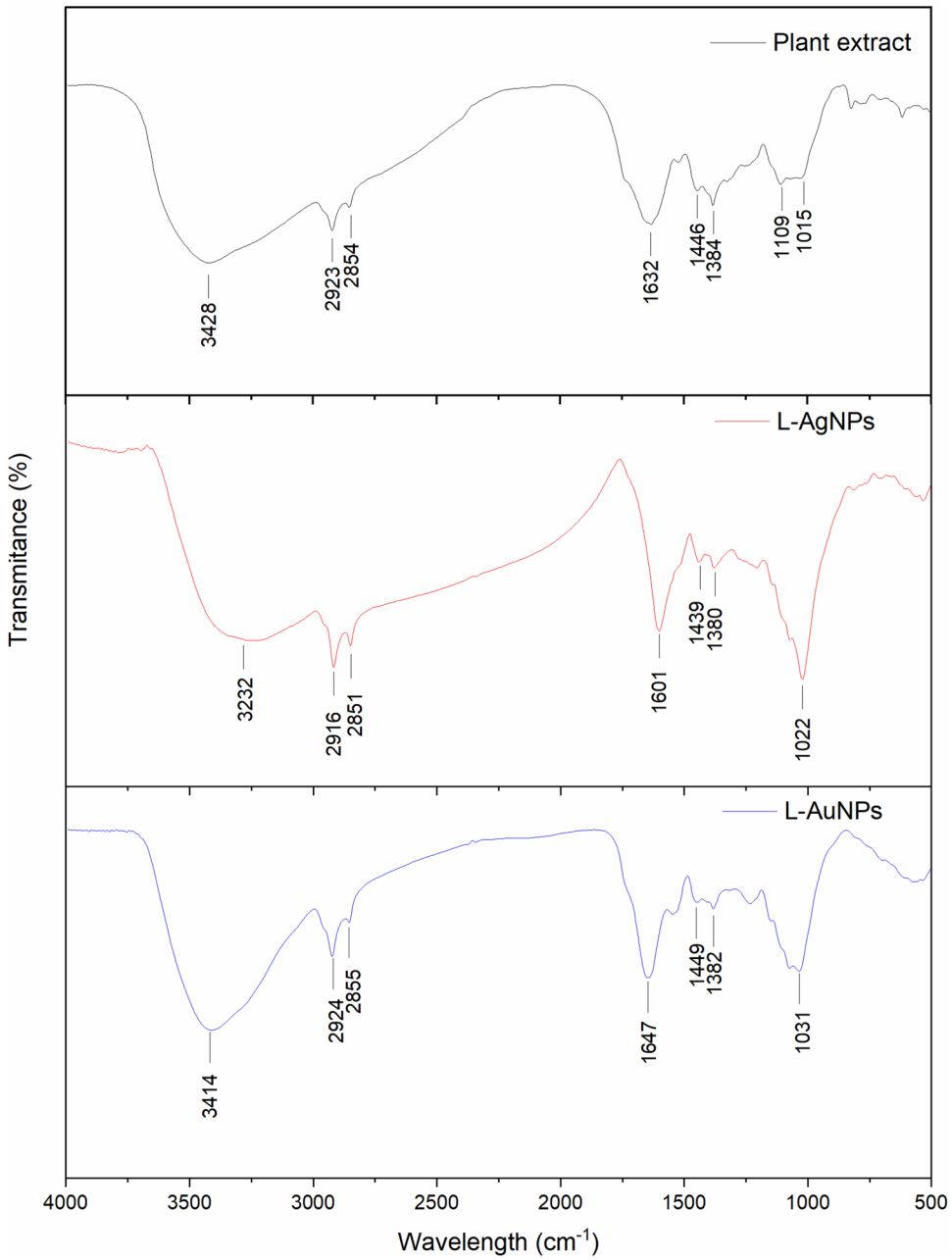

Fig. 3 FT-IR spectra of *L. indica* extract, L-AgNPs and L-AuNPs

range of 5.0–27.5 nm with an average size of 13.5 nm. The AgNPs are highly crystalline as shown in SAED pattern and HRTEM image (Fig. 5c) which showed clear lattice fringe spacing of 0.22 nm, attributed to the (111) plane of the nanoparticles. Meanwhile, L-AuNPs showed an uneven geometry with spherical, triangular and hexagonal shapes. The results revealed a narrow particle size distribution of 7.0–19.0 nm with an average particle size of 14.5 nm. Difference in shape and size of the nanoparticles can be due to different phytochemicals as stabilization agents and reduction potentials of metallic ions. A similar result was also observed for reduction of the metallic ions using other plants [24, 25]. The SAED pattern of AuNPs (Fig. 6c) showed circular rings with clear and bright spots from inner to outer, which might be indexed as (111), (200), (220) and (311) reflections respectively, confirmed FCC structure of MNPs.

The EDX spectra depicted in Figs. 5d and 6d, showed the highest signal at 2.98 keV for the L-AgNPs and three strong signals at 2.13, 8.45 and 9.73 keV for the L-AuNPs. EDX data showed that average content of the silver element (75.50%, w/w) is greater than that of the gold element (55.83%, w/w) in the corresponding nanoparticles. The other peaks corresponding to carbon and oxygen present in both the MNPs may come from the phytochemicals capping onto the AgNPs and AuNPs.

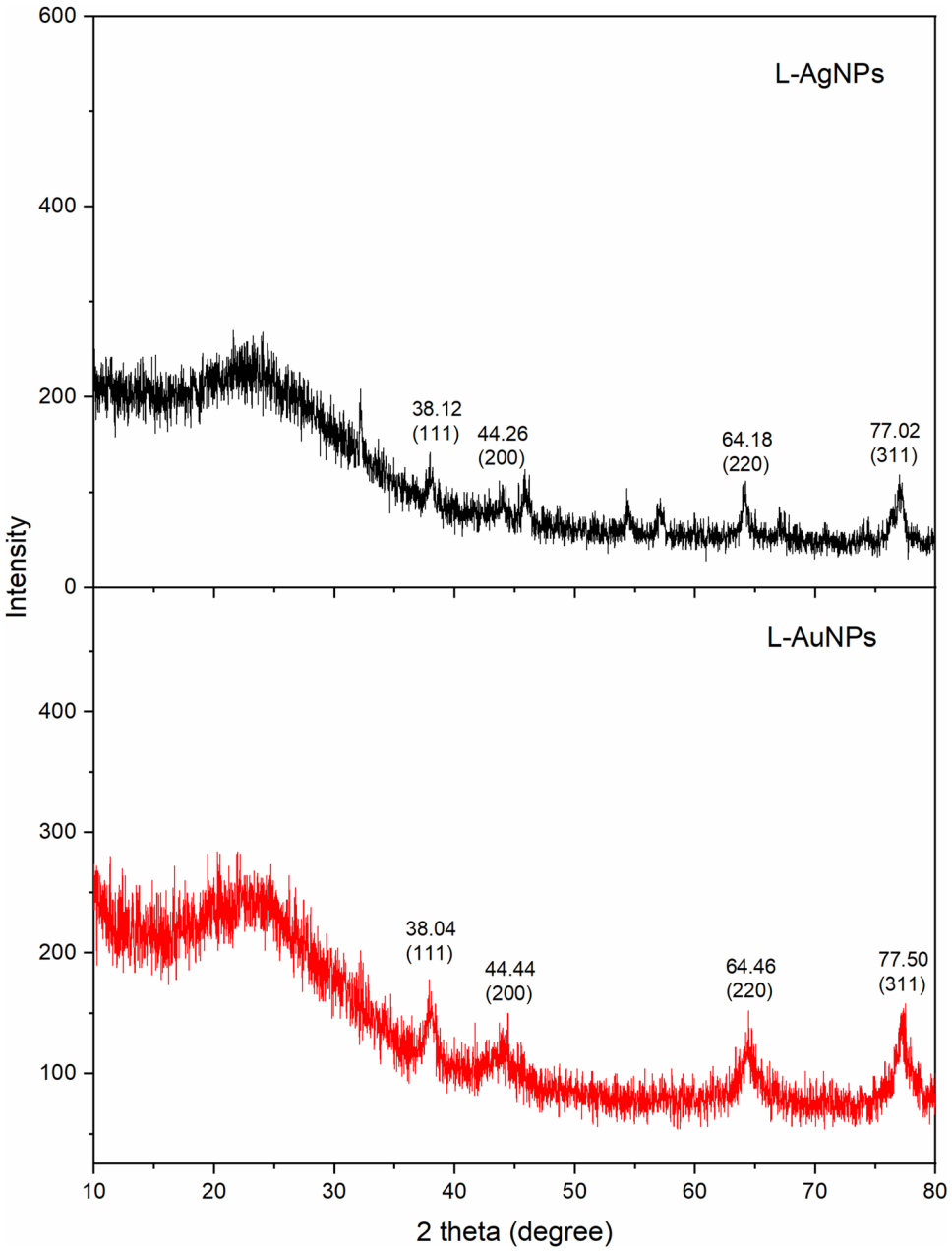

Fig. 4 XRD pattern of synthesized L-AgNPs and L-AuNPs

3.6 Thermal Behaviors

For evaluation of thermal behaviors, simultaneous measurement of TG–DTA curves of the biosynthesized MNPs is performed under the air atmosphere at 20 mL/min and the heating rate of 10 °C/min. The same weight of the solid samples was used for analysis. The significant difference between two nanoparticles was clearly observed in Fig. 7. The data showed that the thermal stability of L-AgNPs (220 °C) is higher than that of L-AuNPs (57 °C). Initial weight loss of L-AgNPs was 3.0% (220–281 °C) while a much high value (9.0%) in temperature range of 57–252 °C was found for L-AgNPs sample. After this period, thermal decomposition of L-AgNPs sample occurs in the second stage accounted about 15.0% between 281 and 464 °C while this stage of the L-AuNPs sample was as high as 50.0% between 252 and 491 °C. Total weight loss of L-AgNPs and L-AuNPs was accounted approx. 18.0% and 59.0%, respectively. Hence, total amount of MNPs presented in the samples can estimate from TG data about 82.0% for AgNPs and 41.0% for AuNPs that are slightly different from the calculation from EDX spectra. Thermal decomposition of the biosynthesized MNPs is probably due to pyrolysis of organic molecules on their surface. DTA curve showed that exothermic reactions occurred at maximum peak of 324 °C for L-AgNPs and at peaks 330 °C and 348 °C for L-AuNPs, attributed

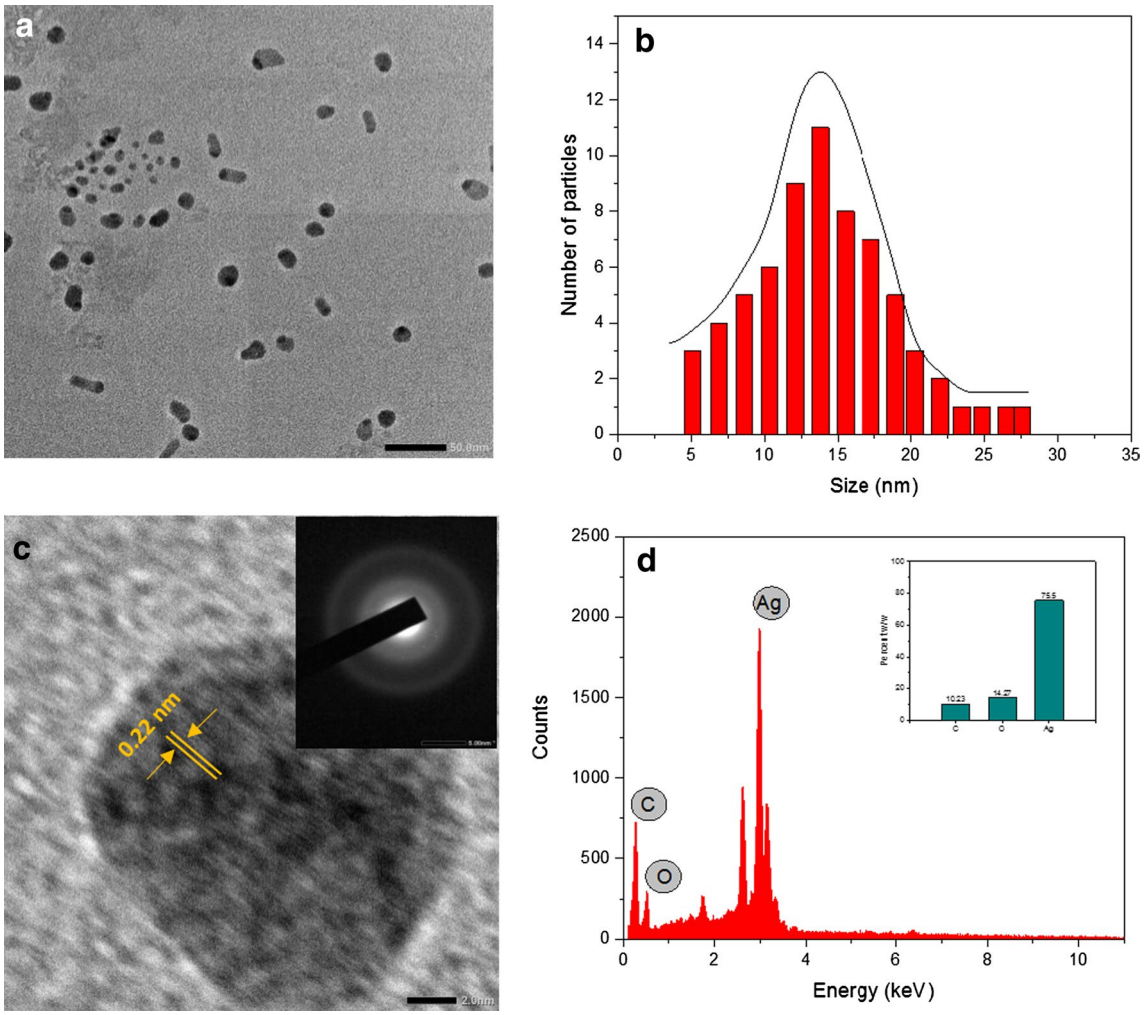

Fig. 5 **a** TEM image, **b** particle size distribution, **c** HRTEM and SEAD pattern (inset), **d** EDX spectrum with average content of elements (inset) of L-AgNPs

to oxidation of organic compounds. The thermal behavior of the organic molecules on surface of the biosynthesized MNPs indicates that the *L. indica* leaf extract is responsible for the reduction of metallic ions and the stabilization of the MNPs.

3.7 Catalytic Performance of Nanoparticles

Water pollution from dyeing industry is the matter of great concern due to its adverse effects on human health, animals and life environments. Thus, treatment of dye pollutant from industrial wastewater is very considerable. This study investigated catalytic activity of MNPs for degradation of 4-NP and MO using aqueous solution of $NaBH_4$ as a model reaction. The previous reports revealed that degradation reaction rate without the catalyst is very slow although it is well known as a thermodynamically favorable reaction [26]. Large oxidation–reduction potential difference between donor and acceptor molecules leads to kinetic barrier and reducing the feasibility of this degradation reaction. To overcome the kinetic barrier, the noble metal nanoparticles such as AgNPs and AuNPs can be used to catalyze the reaction.

The solution of 4-NP exhibited yellow color with absorption maxima at 318 nm. Addition of $NaBH_4$ did not lead to the reducing reaction but color of solution changed to intense yellow. The absorption peaks were shifted to 400 nm confirmed formation of 4-nitrophenolate ions in the alkaline medium (Fig. S2). When the nanoparticles were added to the mixture, reduction of 4-NP started immediately. It can be recognized the solution turned colorless. The UV–Vis curves showed that absorbance at 400 nm decreased progressively with simultaneous appearance of a new peak at around 230 nm which is associated with 4-aminophenol (4-AP) [27, 28]. The reduction of 4-NP into 4-AP completed within 26 min in presence of L-AgNPs and 50 min in presence of L-AuNPs. In the mechanism of 4-NP degradation,

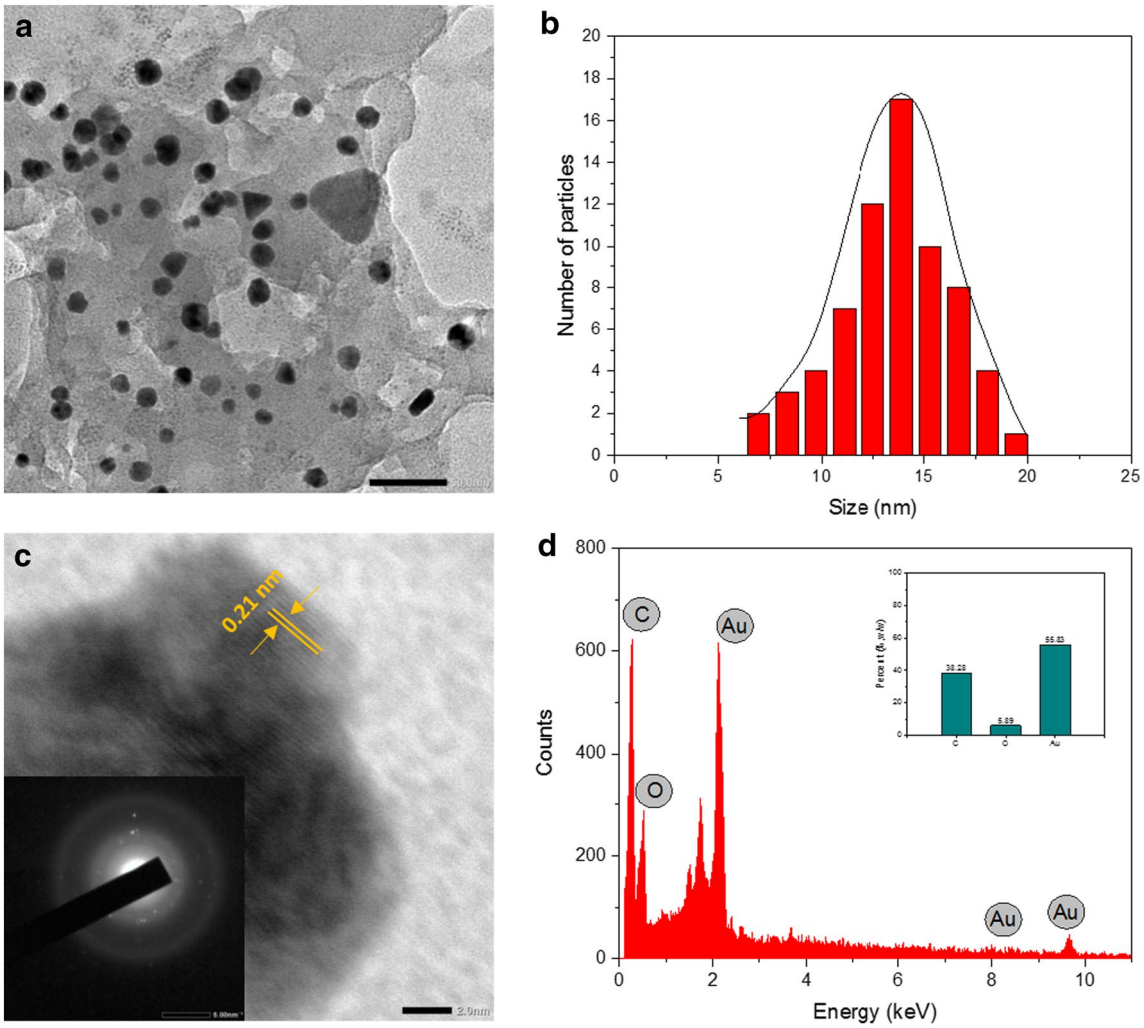

Fig. 6 **a** TEM image, **b** particle size distribution, **c** HRTEM and SEAD pattern (inset), **d** EDX spectrum with average content of elements (inset) of L-AuNPs

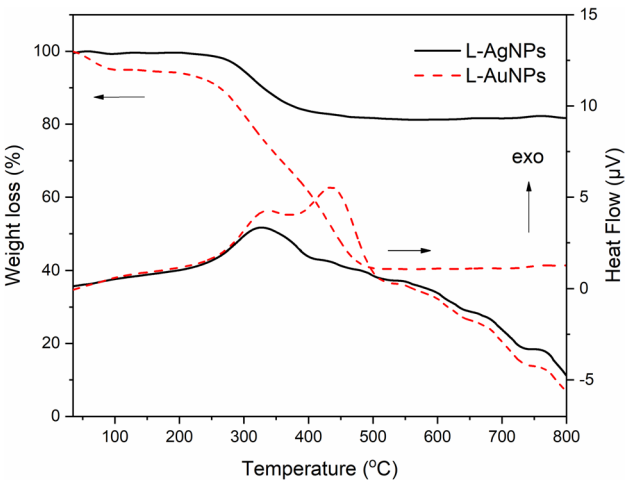

Fig. 7 Simultaneous TG and DTA curves of L-AgNPs and L-AuNPs under the air flow at 20 mL/min and heating rate of 10 °C/min

MNPs play a crucial role for electron transfer. The donor ions BH_4^- are adsorbed at active sites of MNPs surface and then transfer the electron to the acceptor 4-NP molecule forming into the product 4-AP (Fig. 8) [29–31].

For investigation of reaction kinetics, the degradation rates were measured from the plots between $\ln(A_t/A_0)$ and time (s). A linear relationship was found, indicating that the reduction followed pseudo-first order kinetics (Fig. 9). Catalytic performance of L-AgNPs with rate constant (2.1×10^{-3} s^{-1}) was higher than that of L-AuNPs (1.3×10^{-3} s^{-1}). The difference in catalytic activity between two biosynthesized MNPs can relate to content and electron-transferred capacity of corresponding MNPs in the samples.

MO is an azo dye with long chains of conjugation which allows it to be chromophores. MO is largely used for dyeing textiles as artificial color and for acid–base indicator. UV–Vis spectrum of MO in aqueous solution shows peak at

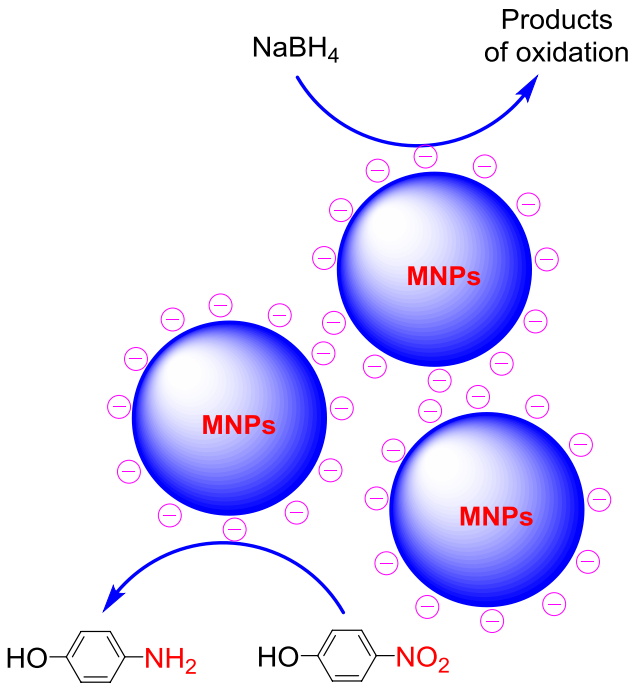

Fig. 8 Proposed mechanism for catalytic degradation of 4-nitrophenol by $NaBH_4$ in presence of MNPs

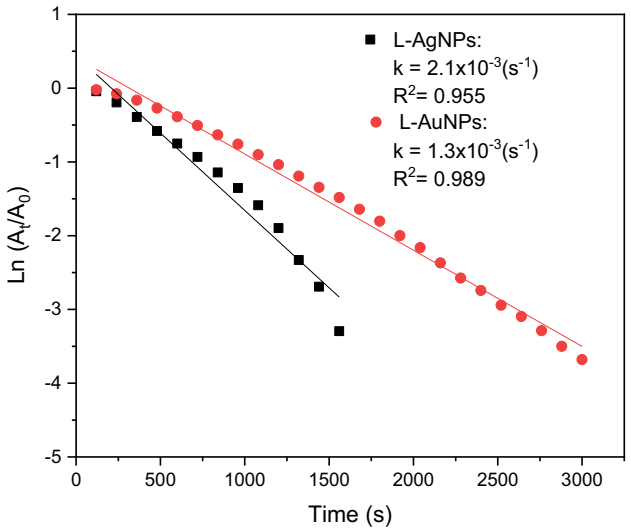

Fig. 9 First order kinetics plotted for degradation of 4-NP in catalysts of L-AgNPs and L-AuNPs

463 nm related to transition of the azo group. The degradation of MO carried out in the MNPs catalyst was observed by using UV–Vis spectra. A steady decrease of the absorbance value of MO was observed and the reduction reaction completed in 16 min for L-AgNPs catalyst and 28 min for L-AuNPs catalyst (Fig. S3). The kinetics of the degradation was studied spectrophotometrically by examining the

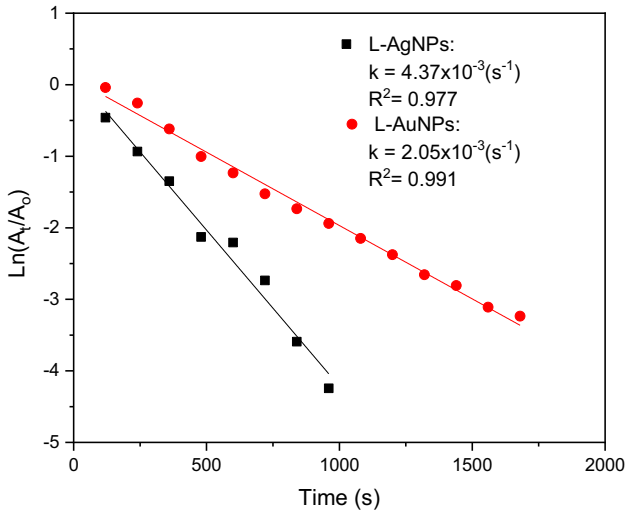

Fig. 10 First order kinetics plotted for degradation of MO in catalysts of L-AgNPs and L-AuNPs

absorbance of peak at 463 nm. The plots of ln $[A_t]/[A_0]$ versus time give straight lines, and rate constants can be calculated directly from the slope of the lines. The data of the first order kinetics are given in the Fig. 10. The rate constant of the MO degradation in presence of L-AgNPs (4.37×10^{-3} s^{-1}) is double that of L-AuNPs catalysis (2.05×10^{-3} s^{-1}).

Catalytic activity of MNPs is dependent on size, morphology and composition of capping agents. Normalized rate constants (k_{nor}) calculated from rate constant per 1 mg of catalyst are often used to compare their catalytic activity [32–34]. The different catalytic systems for degradation of 4-NP and MO are listed in Table 1. MNPs in the present work showed high catalytic performance in comparison from the literatures. For degradation of 4-NP, activity of L-AuNPs is 10-fold as much as that based on *C. religiosum* gum while L-AgNPs showed a fivefold increase in comparison with AgNPs prepared from *D. longan* seed. Also, L-MNPs displayed much higher catalytic activity for MO degradation. It indicated that *L. indica* leaf is an excellent source for fabrication of MNPs that can efficiently apply in the field of pollutant degradation.

4 Conclusions

Based on the aqueous extract of *L. indica* leaf, AgNPs and AuNPs were successfully biosynthesized without using any toxic and expensive chemical agents. This work demonstrated that the catalytic MNPs can be effectively prepared by a simple and low-cost method. The colloidal L-AgNPs with a spherical shape and L-AuNPs with multi shapes well dispersed in the solution. The biogenic MNPs displayed the

Table 1 Comparison of normalized rate constant of different photocatalytic systems for the degradation of 4-nitrophenol and methyl orange

Pollutants	MNPs	Biological system	Size (nm)	K_{nor} (s^{-1} mg^{-1})	References
4-NP	AgNPs	*D. longan* seed	40	4.7×10^{-4}	[35]
	AuNPs	*C. religiosum* gum	6.9	1.27×10^{-4}	[36]
	PdNPs	*D. regia* Leaf	2–4	2.33×10^{-3}	[37]
	AgNPs	*L. indica* leaf	13.5	2.1×10^{-3}	This work
	AuNPs	*L. indica* leaf	14.5	1.3×10^{-3}	This work
MO	AuNPs	*A. nigra* leaves	21.5	4.4×10^{-5}	[38]
	AuNPs	*D. coromandeliana* roots	10.5	1.7×10^{-3}	[39]
	AgNPs	*L. indica* leaf	13.5	4.37×10^{-3}	This work
	AuNPs	*L. indica* leaf	14.5	2.05×10^{-3}	This work

enhanced catalytic activities in the degradation reactions which can provide a vast application in eco-friendly environmental decomposition of organic pollutants.

Acknowledgements This research is funded by Vietnam National Foundation for Science and Technology Development (NAFOSTED) under Grant No. 104.99-2018.369.

Compliance with Ethical Standards

Conflict of interest The authors declare that they have no conflict of interest.

References

1. P.K. Jain, X. Huang, I.H. El-Sayed, M.A. El-Sayed, Acc. Chem. Res. **41**, 1578 (2008)
2. A. Schrofel, G. Kratošová, I. Šafařík, M. Šafaříková, I. Raška, L.M. Shor, Acta Biomater. **10**, 4023 (2014)
3. J. Biswal, S.P. Ramnani, S. Shirolikar, S. Sabharwal, Radiat. Phys. Chem. **80**, 44 (2011)
4. J.D. Mackenzie, E.P. Bescher, Acc. Chem. Res. **40**, 810 (2007)
5. A. Shahzad, H. Saeed, M. Iqtedar, S.Z. Hussain, A. Kaleem, R. Abdullah, S. Sharif, S. Naz, F. Saleem, A. Aihetasham, A. Chaudhary, J. Nanomater. (2019). https://doi.org/10.1155/2019/5168698
6. Y. Xu, Y. Hou, Y. Wang, Y. Wang, T. Li, C. Song, N. Wei, Q. Wang, Ecotoxicol. Environ. Saf. **168**, 356–362 (2019)
7. S. Ahmed, M. Ahmad, B.L. Swami, S. Ikram, J. Adv. Res. **7**, 17 (2016)
8. Q. Zhou, M. Zhou, Q. Li, R. Wang, Y. Fu, T. Jiao, Colloids Surf. A **567**, 69 (2019)
9. R. Sood, D.S. Chopra, Phytomedicine **50**, 148 (2018)
10. M.K. Choudhary, J. Kataria, S. Sharma, Appl. Nanosci. **7**, 439 (2017)
11. N.K.R. Bogireddy, H.A.K. Kumar, B.K. Mandal, J. Environ. Chem. Eng. **4**, 56 (2016)
12. S. Phukan, P. Bharali, A.K. Das, M.H. Rashid, RSC Adv. **6**, 49307 (2016)
13. B. Bonigala, B. Kasukurthi, V. Viswanath Konduri, U.K. Mangamuri, R. Gorrepati, S. Poda, Environ. Sci. Pollut. R. **25**, 32540 (2018)
14. S.Y. Wang, H.N. Chang, K.T. Lin, C.P. Lo, N.S. Yang, L.F. Shyur, J. Agric. Food Chem. **51**, 1506 (2003)
15. Y.H. Chen, H.Y. Chen, C.L. Hsu, G.C. Yen, J. Agric. Food Chem. **55**, 1743 (2007)
16. C.I. Choi, H.J. Eom, K.H. Kim, Russ. J. Biorgan. Chem. **42**, 310 (2016)
17. Y. Liu, Y. Zhang, Q. Kou, Y. Chen, Y. Sun, D. Han, D. Wang, Z. Lu, L. Chen, J. Yang, S.G. Xing, Nanomaterials **8**, 329 (2018)
18. K.H. Kim, K.H. Lee, S.U. Choi, Y.H. Kim, K.R. Lee, Arch. Pharm. Res. **31**, 983 (2008)
19. S. Joseph, B. Mathew, Spectrochim. Acta A **136**, 1371 (2015)
20. C.I. Choi, H.J. Eom, K.H. Kim, Russ. J. Biorgan. Chem. **42**, 310 (2016)
21. Y.H. Chen, H.Y. Chen, C.L. Hsu, G.C. Yen, J. Agric. Food Chem. **55**, 1743 (2007)
22. K. Jeeva, M. Thiyagarajan, V. Elangovan, N. Geetha, P. Venkatachalam, Ind. Crops Prod. **52**, 714 (2014)
23. K. Anandalakshmi, J. Venugobal, V. Ramasamy, Appl. Nanosci. **6**, 399 (2016)
24. T.T.N. Nguyen, T.T. Vo, B.N.H. Nguyen, D.T. Nguyen, V.S. Dang, C.H. Dang, T.D. Nguyen, Environ. Sci. Pollut. Res. **25**, 34247 (2018)
25. S. Francis, E.P. Koshy, B. Mathew, Bioprocess Biosyst. Eng. **41**, 939 (2018)
26. T.D. Nguyen, C.H. Dang, D.T. Mai, Carbohydr. Polym. **197**, 29 (2018)
27. Y.S. Seo, E.Y. Ahn, J. Park, T.Y. Kim, J.E. Hong, K. Kim, Y. Park, Y. Park, Nanoscale Res. Lett. **12**, 7 (2017)
28. E. Menumerov, R.A. Hughes, S. Neretina, Nano Lett. **16**, 7791 (2016)
29. Y. Liu, Y.Y. Zhang, Q.W. Kou, Y. Chen, D.L. Han, D.D. Wang, Z.Y. Lu, L. Chen, J.H. Yang, S. Xing, RSC Adv. **8**, 2209 (2018)
30. W. Wang, Y. Kang, A. Wang, J. Nanopart. Res. **16**, 2281 (2014)
31. T.D. Nguyen, T.T. Vo, C.H. Nguyen, V.D. Doan, C.H. Dang, J. Mol. Liq. **276**, 927 (2019)
32. H. Huang, Z. Zhao, W. Hu, C. Liu, X. Wang, Z. Zhao, W. Ye, J. Taiwan Inst. Chem. E **84**, 101 (2018)
33. J. Song, Y. Zhu, J. Zhang, J. Yang, Y. Du, W. Zheng, C. Wen, Y. Zhang, L. Zhang, Langmuir **35**, 1563 (2019)
34. L. Sun, P. Lv, H. Li, F. Wang, W. Su, L. Zhang, J. Mater. Sci. **53**, 15895 (2018)
35. F.U. Khan, Y. Chen, N.U. Khan, Z.U.H. Khan, A.U. Khan, A. Ahmad, K. Tahir, L. Wang, M.R. Khan, P. Wan, J. Photochem. Photobiol., B **164**, 344 (2016)
36. S. Maity, I. Kumar, S. Syed, S. Islam, Phys. E Low Dimens. Syst. Nanostruct. **45**, 130 (2012)
37. P. Dauthal, M. Mukhopadhyay, Ind. Eng. Chem. Res. **52**, 18131 (2013)
38. D. Baruah, M. Goswami, R.N.S. Yadav, A. Yadav, A.M. Das, J. Photochem. Photobiol., B **186**, 51 (2018)
39. C. Umamaheswari, A. Lakshmanan, N.S. Nagarajan, J. Photochem. Photobiol., B **178**, 33 (2018)